

Cavitating structures at inception in turbulent shear flow

Karuna Agarwal; Omri Ram; Joseph Katz*

Department of Mechanical Engineering, The Johns Hopkins University, Baltimore, Maryland 21218

Abstract

Cavitation inception in the near field of turbulent shear layers occurs along secondary quasi-streamwise vortices developing between the primary spanwise vortices. To observe these incepting structures and understand the flow conditions under which they form, the present paper compares the flow statistics to results of high speed imaging performed in the shear layer behind a backward facing step. Simultaneous top and side imaging captures the location and spatial arrangement of the cavitating structures at varying cavitation indices. Two-dimensional PIV measurements characterize the mean velocity and Reynolds stress profiles, for Reynolds numbers in the separating boundary layer of $Re_\tau = 807, 1504, 2345$. Being concentrated within the quasi-streamwise strings, the cavitation events are preferentially located in the near field of the shear layer, where the unsteady flow is dominated by coherent structures, upstream of the peaks in turbulence level. They move more upstream with increasing Re and decreasing pressure. Furthermore, the probability of cavitation increases by 3-5 times when the velocity is increased from 10.5 to 16 m/s. These indicate that the pressure fluctuation peaks causing the cavitation do not follow the same trends as the Reynolds stresses which collapse when scaled by the freestream velocity.

Keywords: cavitation inception; turbulent shear layer; flow structure visualization

1. Introduction

Cavitation, being one of the fundamental phenomena that affect the efficiency, noise, and life expectancy of hydrodynamic devices, has been studied extensively throughout the last century. However, much of the basic mechanisms that lead to the inception of cavitation, the growth rate of cavities and their coupling with the surrounding flow, is yet to be understood; especially for cases involving turbulent shear flows. Previous studies, e.g. [1-4], have shown that the cavitation inception index typically increases with Reynolds number. Furthermore, while the inception process is intermittent, depending on the distributions of nuclei and low-pressure sites, cavitation appears in quasi streamwise vortices at higher ambient pressures compared to events occurring in the larger spanwise vortices. Hence, the elongated vortices developing between the spanwise structures must have lower core pressure in spite of their much lower strength. The location and the number of these axial vortices vary, but they migrate upstream with increasing Reynolds number and have preferred spanwise locations [5]. Little is known about the location and strength of these structures, hence, data that would enable prediction of cavitation inception in them is still lacking. More recent work [6,7] on turbulence-cavitation interactions have focused at developed stages of cavitation. The aim of this study is to characterize the structure of early phases of cavitation in a shear layer developing downstream of a backward facing step and relate it to the local flow and turbulence fields. It is the first step in an effort to relate the pressure field and nuclei distributions on cavitation inception.

Experimental set-up

The experiments have been conducted in a water tunnel facility described in [8]. It has a 63.5×50.8 mm test section and a maximum velocity of 18 m/s. The flow is driven by a pair of centrifugal pumps located 5 m below the test section and passes through a 1000-liter buffer tank before entering the settling chamber leading to the test section. The geometry used to generate a free shear layer downstream of a backward-facing step is illustrated in figure 1. The step height is 10 mm, and the expansion ratio is 1.19. The shape of the nozzle is a fifth-order polynomial to ensure that the curvature is nearly zero at both ends to prevent undesirable pressure gradients. Grooves machined at bottom of the entrance to the test section are used for tripping the boundary layer, ensuring that all the present tests are performed when the separating boundary layer is turbulent.

Two-dimensional PIV is used for characterizing the flow field without cavitation, from the boundary layer all the way to the reattachment region. The flow is seeded with $2 \mu\text{m}$ silver-coated glass particles, the light sheet is generated

*Corresponding Author, Joseph Katz: katz@jhu.edu

using a Quantel Evergreen Nd:YAG laser, images are recorded by a 6600×4400 pixels Imperx BB640 camera equipped with 105 mm Nikon Micro lens for slightly overlapping 36.3×24.2 mm ($x \times y$) sample areas (Figure 1). Cross-correlation analysis using the Davis software package with 32×32 pixels interrogation areas, with 75% overlap between windows, generates 827×552 vector arrays with spacing of 43 μm . About 2000 realizations are used to obtain the mean flow and Reynolds stress statistics. Experiments have been performed at three free-stream velocities, 5.3, 10.5 and 16 m/s.

The setup used for high speed imaging of the cavitating structures is also illustrated in figure 1. Two synchronized orthogonal views, side and top views, are used for capturing all three dimensions of the cavitation bubbles. The images are recorded at 3931.8 fps for 2.56 seconds at the resolution of 1730×730 using pco.Dimax cameras. Two halogen lamps are used for back-lighting the test section, enabling an exposure time of 3.98 μs . The dissolved oxygen content is kept close to 4.5ppm, representing 70-120% of the saturation level in the test section, as measured using an optical dissolved oxygen sensor (FireStingO2). The mean pressure is measured at the inlet to the test section, and the pressure above the step is inferred using the Bernoulli's equation.

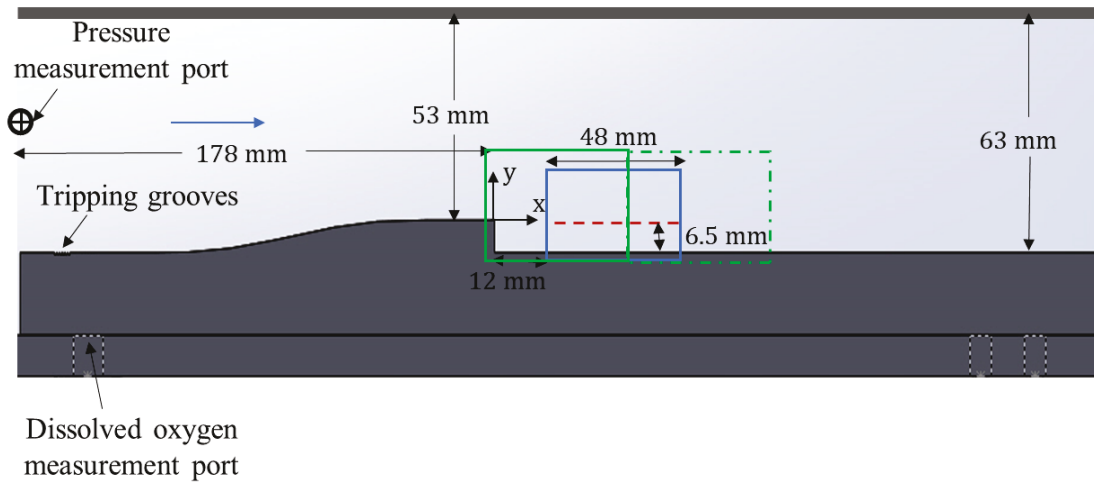


Figure 1: Setup for 2D PIV and visualizations experiments. The fields of view for PIV are marked in green, field of view of the side camera blue and the focal plane of the top camera in red.

2. Results and discussion:

2.1. 2D PIV results

A normalized plot of the boundary layer profile at three free-stream velocities is presented in figure 2(a). The wall shear velocity $u_\tau = \sqrt{\tau_{wall}/\rho}$ is estimated by least square fitting to the velocity profile in the log layer, and the boundary layer height δ is determined based on the elevation of peak velocity. The resulting $Re_\tau = u_\tau \delta / \nu$ are 807, 1504 and 2345 for free stream velocities U of 5.3 m/s, 10.5 m/s and 16 m/s, respectively. The reattachment length x_r determined based on the point where the zero velocity line in the shear layer reaches the surface, is found to decrease with increasing velocity, from 61.9, to 55.3 mm, and to 53.1 mm. As demonstrated in Figure 2(b) the mean velocity profiles collapse after normalizing the horizontal axis by x_r and the vertical axis by h (step height). The sample profile in Figure 2(c) show that the two normal and one shear Reynolds stress components also nearly collapse using the same length scales and the freestream velocity. This figure also indicates that the freestream turbulence intensity for all cases falls below 1%. For reference, Figure 2(d) displays sample contour plots of $\overline{u_x u_y} / U$ and $\overline{u_y u_y} / U$. The slight mismatch occurring at $x \sim 33\text{mm}$ corresponds due to the stitching of two PIV data sets. As is evident, $\overline{u_y u_y} / U$, which in boundary layers correlates well with the pressure fluctuations [9], increase with x/x_r , peaking at 0.95, far downstream of the cavitation inception area described below.

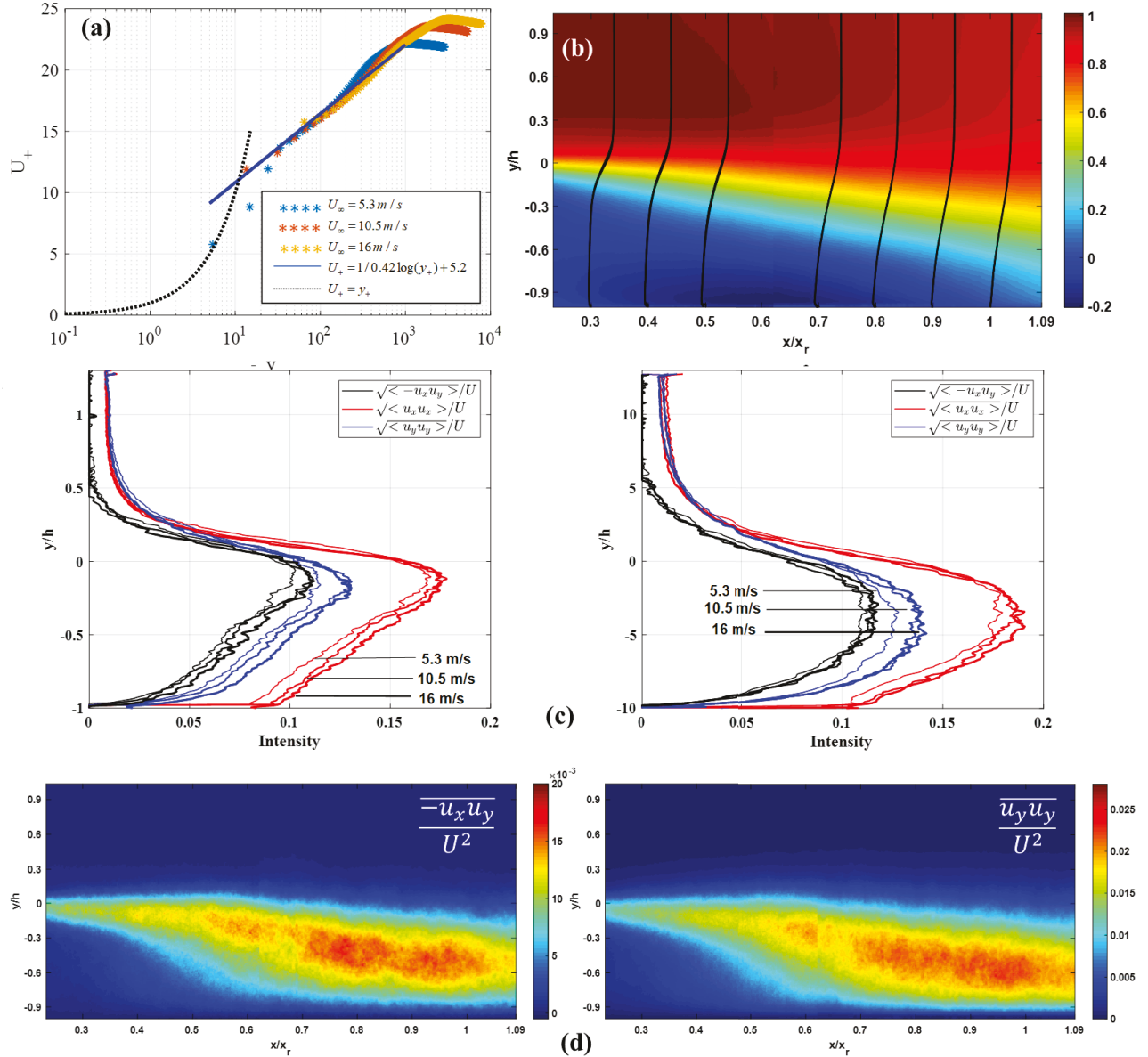


Figure 2 (a) The scaled velocity profile of the separating turbulent boundary layer and the fitted log function. (b) Average velocity profile scaled with U and x_r . (c) Turbulent fluctuation quantities scaled with free-stream velocity at $x/x_r = 0.5$ (left) and $x/x_r = 0.7$ (right). (d) Mean square wall-normal fluctuations and Reynolds stress.

2.2. Cavitation imaging

Figure 3 presents a set of sample snapshots showing the time evolution of a cavitation event where a free stream bubble (circled on the leftmost image), rapidly expand into an elongated quasi-streamwise cavity. Between the first two exposures, the bubble grows to nearly its full length ($>5 \text{ mm}$) in less than $250 \mu\text{s}$, indicating the present frame rate is too slow to capture the cavitation inception. Moreover, the entire life span of the cavitation event is about 2 ms , during which the bubble grows along inclines the streamwise direction with small changes in its radius, and then fragments into small bubbles, before disappearing (at least in the present magnification). The relationship between these phenomena and the transient dynamics of secondary vortices developing between the primary spanwise structures in the shear layer is yet to be well understood. Interestingly, the length of these cavities does not seem to change significantly with cavitation index and freestream velocity.

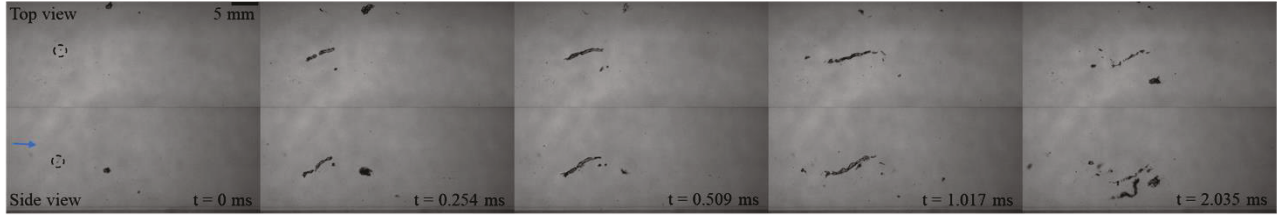


Figure 3: Time evolution of a cavitating bubble seen in two views. The nuclei marked in $t = 0$ ms, explodes along the streamwise direction in 0.254 ms and collapses by $t = 2.035$ ms. The freestream velocity is 10.5 m/s and the cavitation index 0.39.

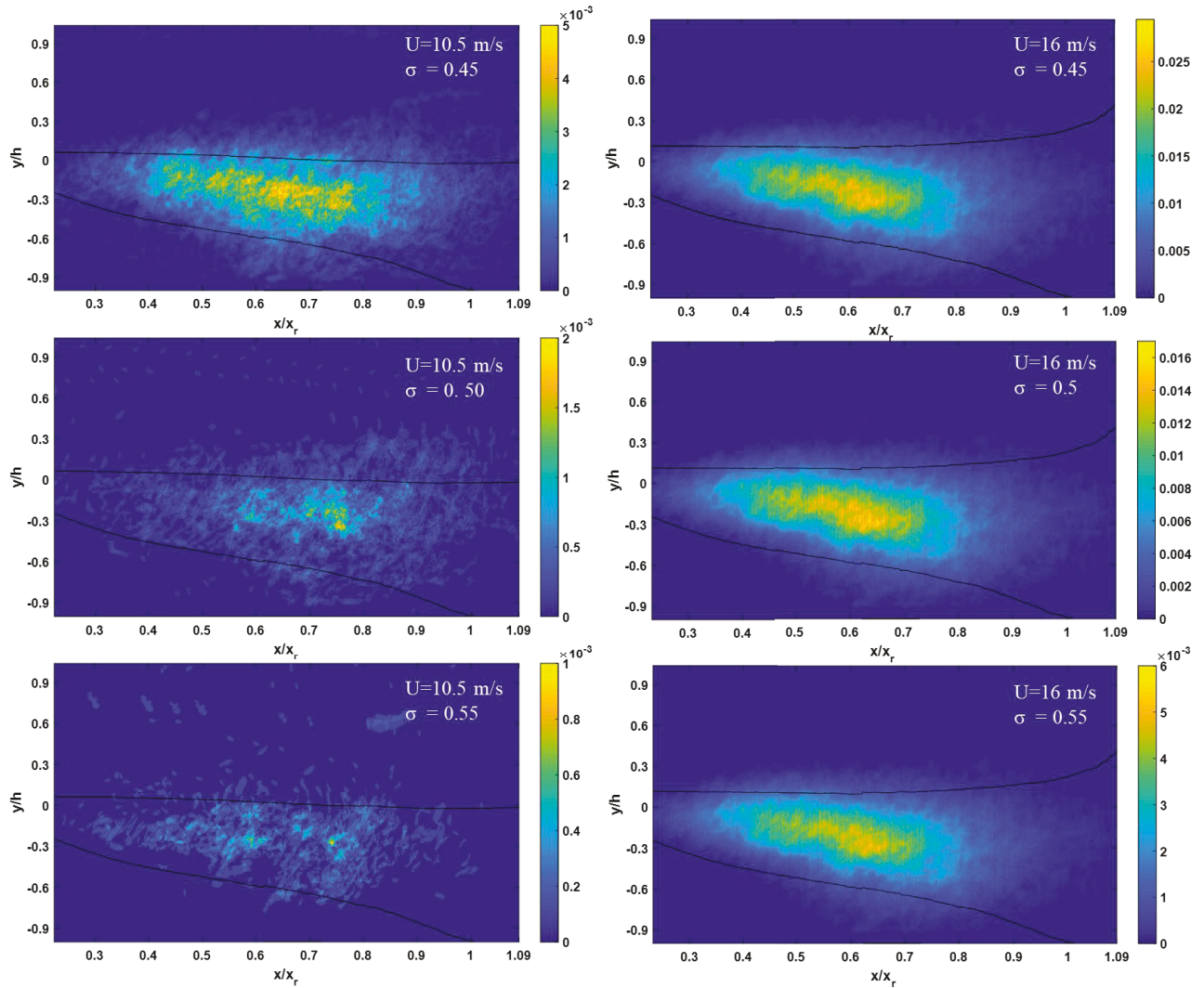


Figure 4: The probability of an elongated bubble ($\frac{major}{minor} = 2$) to be at a given location for velocities 10.5 m/s and 16 m/s and cavitation index 0.45, 0.5 and 0.55. The black lines represents 0 and $0.9U$ average velocity contours.

As a first step to characterize the behavior of these cavities, six set of 10000 images each of early phases of cavitation have been examined to determine the preferred location of the elongated bubbles. Only bubbles larger than $157 \mu\text{m}$ are accounted for. If the analysis is performed after imposing a ratio of major to minor axes of more than 2.0, the results are not significantly different, indicating that overwhelmingly, most of the bubbles are elongated structures. The time averaged 2D projected signatures of these bubbles are normalized with the total number of frames to represent the probability of having cavitation at a certain location. The results are mapped in Figure 4 (note the

different scales) for two velocities and three cavitation indices $\sigma = 2(P - P_v)/\rho U^2$, where P is the mean pressure above the step, and P_v is the vapor pressure at the water temperature. As is evident, cavitation is most likely to take place at $0.5 < x/x_r < 0.75$. As indicated by the vertically averaged probability plots, for both velocities, the most probable site moves upstream with increasing velocity (Figure 5). The axial locations of these probability peaks also do not coincide with those of the peaks in Reynolds stresses.

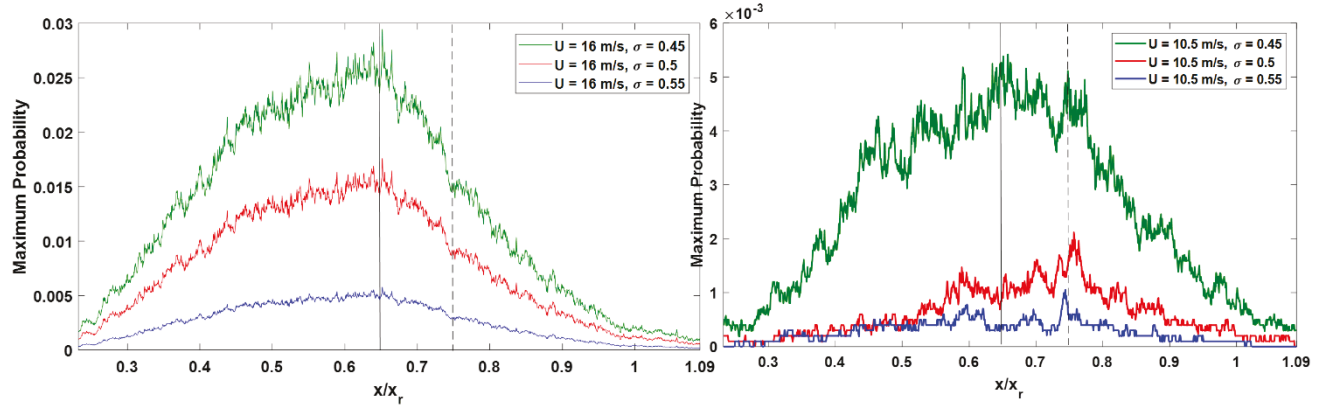


Figure 5. Vertically collapsed maximum probability plots for the six cases, higher velocity case on the left. The solid black line indicates the location of maximum probability for 16 m/s velocity and the dashed line for 10.5 m/s.

As expected, the likelihood of cavitation occurrence increases with decreasing cavitation index. However, there is 3-5 times increase in the probability of cavitation inception as the velocity is increased from 10.5 to 16 m/s for the same cavitation index. This trend contrasts with the collapse of Reynolds stresses under the same conditions, further indicating that the pressure fluctuation *peaks* causing the cavitation do not follow the same trends as the Reynolds stresses. Finally, spatially averaging the probability at $0.45 < x/x_r < 0.8$ shows that its magnitude increases faster than the increase in cavitation index. These findings provide motivation for measuring the scaling trends of the pressure field within the quasi streamwise vortices in the shear layer.

3. Conclusion

The present study compares the scaling trends of the most likely location of early phases cavitation to those of the Reynolds stresses in the shear layer downstream of a backward facing step. The cavitation is most likely to take place at $0.45 < x/x_r < 0.75$, moving upstream with decreasing cavitation index and increasing velocity. Unlike the Reynolds stresses, which collapse when scaled using the free stream velocity, the likelihood of cavitation increases by 3-5 times as the velocity increases from 10.5 to 16 m/s. Hence, the pressure fluctuation *peaks* associated with the quasi streamwise structures causing the early cavitation do not follow the same trends as the turbulence in the shear layer. These findings provide the motivation for a systematic study of the pressure field generated by primary and secondary vortices in the shear layer. Fortunately, recent advances in technique for determining the instantaneous pressure distributions in turbulent flows based on data obtained from time-resolved three dimensional velocity measurements makes such a task feasible [10,11].

References

- [1] Katz, J. (1984). *Cavitation phenomena within regions of flow separation*. Journal of Fluid Mechanics, 140.
- [2] Katz, J., & O'hern, T. J. (1986). *Cavitation in large scale shear flows*. Journal of fluids engineering. 108(3).
- [3] O'hern, T. J. (1990). *An experimental investigation of turbulent shear flow cavitation*. Journal of fluid mechanics, 215.
- [4] Gopalan, S., Katz, J., & Knio, O. (1999). *The flow structure in the near field of jets and its effect on cavitation inception*. Journal of fluid mechanics, 398.
- [5] Bernal, L. P., & Roshko, A. (1986). *Streamwise vortex structure in plane mixing layers*. Journal of Fluid Mechanics, 170.
- [6] Iyer, C. O., & Ceccio, S. L. (2002). *The influence of developed cavitation on the flow of a turbulent shear layer*. Physics of fluids, 14(10).

- [7] Aeschlimann, V., Prothin, S., Barre, S., & Djeridi, H. (2012). *High speed visualizations of the cavitating vortices of 2D mixing layer*. European Journal of Mechanics-B/Fluids, 31.
- [8] Gopalan, S., & Katz, J. (2000). *Flow structure and modeling issues in the closure region of attached cavitation*. Physics of fluids, 12(4).
- [9] Joshi, P., Liu, X., & Katz, J. (2014). *Effect of mean and fluctuating pressure gradients on boundary layer turbulence*. Journal of Fluid Mechanics, 748.
- [10] Van Oudheusden, B. W. (2013). *PIV-based pressure measurement*. Measurement Science and Technology, 24(3).
- [11] Wang, Zhang and Katz (2018). *GPU-based, parallel-line, omni-directional integration of the acceleration field to obtain the 3D pressure distribution*. 10th International symposium on cavitation.